Materials Today Chemistry 30 (2023) 101491

Contents lists available at ScienceDirect

Materials Today Chemistry

journal homepage: www.journals.elsevier.com/materials-today-chemistry/

Synthesis optimisation of copper-based layered perovskites as thermal energy storage materials

R. Salgado-Pizarro, C. Barreneche, A.I. Fernández*

Departament de Ciència de Materials i Química Física, Secció de Ciència de Materials, Facultat de Química, Universitat de Barcelona, C/ Martí I Franquès 1-11, Barcelona, 08028, Spain

ARTICLE INFO

Article history:
Received 10 January 2023
Received in revised form
24 February 2023
Accepted 4 March 2023
Available online xxx

Keywords:
Solid-solid phase change materials
Organometallic materials
Polymorphic transitions
Thermal energy storage materials

ABSTRACT

Solid-solid phase change materials (ss-PCMs) are promising materials for thermal energy storage applications because they do not require shape stabilisation or encapsulation. In addition, depending on the ss-PCM used, they can reduce corrosion issues and allow faster charging and discharging. Organometallic ss-PCM, particularly layered hybrid organic-inorganic compounds, have been investigated in this work due to the scientific interest in their potential use as phase change materials to store energy via polymorphic transitions. Here we have assessed the synthesis of $(C_{12}H_{28}N)_2CuCl_4$, a potential material for thermal energy storage. The transition enthalpy and specific heat are the key values to maximise. Two different synthesis procedures were followed: reflux and recrystallisation, and direct synthesis. Three different solvents were also used: methanol, ethanol and isopropanol. In order to find out which processes and solvent media were most promising, the synthesis yield, crystal and molecular structure, and thermal parameters such as transition enthalpy and specific heat were evaluated. Direct synthesis processes produced the most promising material for thermal energy storage due to higher yield and better enthalpy ratio.

1. Introduction

Phase change materials (PCMs) can absorb and release energy during a reversible phase transition, at a constant phase transition temperature. They are normally used for thermal energy storage and temperature regulation. Three types of PCM are associated with the type of phase transition. Solid-solid PCM (ss-PCM), solid-liquid PCM (sl-PCM), and liquid-gas PCM (lg-PCM). The most studied and established are sl-PCM, due to their high energy density and wide range of phase transition temperatures. However, they present some issues, such as low thermal conductivity, corrosion, and leakage [1–3]. Some of these issues are addressed by increasing the thermal conductivity by adding carbon nano-fibre/tubes, graphite nanoplatelets, and graphite oxide, among others [4], and reducing corrosion and leakage by encapsulating or shape stabilizing the sl-PCM [5–9].

Nevertheless, ss-PCM do not need to be encapsulated or shape stabilized for technical use, have fewer corrosion issues, and allow better heat transfer, which means fast charge/discharge of the TES system [10]. There are four types of ss-PCM, referring to the nature of their composition: organic, inorganic, polymeric and organometallic [11,12]. The organometallic ss-PCM has high potential due to its intrinsic properties such as good transition enthalpy, thermal conductivity and chemical and thermal stability, no volume change, and low toxicity [10]. The phase transition temperature of the organometallic ss-PCMs is between 305 K and 433 K, which makes them ideal for use in buildings for thermal regulation, heat recovery in industries, and thermal management in cooling electronics, among other applications.

The organometallic ss-PCM called layered perovskites are the bis(alkylammonium) tetrahalometallates (II) $(C_nH_{2n+1}NH_3)_2MX_4$, where n varies from 8 to 18, M is a divalent transition metal and X is a halogen. The phase transitions of these layered perovskites rely on the motion of the organic part, while the inorganic part remains immobile, as in a crystalline model of the bilayer [13]. Several studies suggest that these organometallic ss-PCMs are suitable for TES [14–16]. It is reported that the layered perovskites CuC_n, MnC_n, ZnC_n and CoC_n present a transition temperature that makes them suitable for TES [14,17,18]. The energy storage capacity of these components is strongly dependent on the length of the alkylamine. The average enthalpy of the first transition of CuC_{12} is ~69 J/g

* Corresponding author.
E-mail address: ana_inesfernandez@ub.edu (A.I. Fernández).

https://doi.org/10.1016/j.mtchem.2023.101491

[13,15,18–20], CuC_{14} is ~73 J/g [13,14], MnC_{12} is ~77 J/g [13,16,18,19,21], MnC_{14} is ~87 J/g [13,14], ZnC_{12} is ~102 J/g [13,14,21–23], ZnC_{16} is ~104 J/g [16,18,24], CoC_{12} is ~78 J/g [18,25] and CoC_{16} is ~114 J/g [18,25].

The typical approach to prepare these compounds is to react between stoichiometric amounts of an alkylamine, metal chloride and hydrochloric acid in absolute ethanol or anhydrous methanol. The solution is then refluxed for 4 h and cooled to allow the precipitation of the desired crystals, then filtered off and recrystallized several times in chloroform, absolute ethanol or anhydrous methanol [14,19,20]. Needham, G.F. and Willet, R.D. perform a two-step synthesis procedure in which the desired alkylamine is dissolved in warm ethanol (95%) and an excess of HCl to obtain the hydrochloride alkylamine. Separately, the metal chloride is dissolved in warm ethanol and the two solutions are mixed together in a 2:1 ratio. After cooling the solution, the solid is obtained [13]. Kan J.K. et al. Prepare the material in a two-step synthesis procedure similar to Needham, G.F and Willet R.D, where firstly the hydrochloride alkylamine is obtained by bubbling gaseous hydrochloric acid through the alkylamine dissolved in benzene and the product is recrystallized and filtered. Secondly, the hydrochloride alkylamine obtained is dissolved in ethanol and mixed with the metal chloride in a stoichiometric ratio and kept under reflux for one day. The final product is then recrystallized twice in absolute ethanol [15]. These reported synthesis procedures are mainly aimed at obtaining a pure crystal.

The main objective of the present study is to evaluate and optimise the synthesis of bis(dodecylammonium) tetrachlorocuprate ($(C_{12}H_{28}N)_2CuCl_4$), also named CuC_{12}, for thermal energy storage. Here, the synthesis of CuC_{12} in different solvent media and recrystallization media is studied to determine the importance of recrystallization for TES applications. In addition, the synthesis yield was evaluated, and a comprehensive morphological, structural and thermal characterization has been carried out to elucidate which synthesis procedure is most promising.

2. Materials and methods

2.1. Materials and reagents

The solvents used for the synthesis were methanol (MetOH) anhydrous for analysis (max. 0.003% H_2O) (Nº CAS 67-56-1) from Merck Group, 2-propanol (IspOH) (max. 0.05% H_2O) (Nº CAS 67-63-0) from VWR international and ethanol (EtOH) 96% (Nº CAS 64-17-5) from Labbox. The reactants used for the synthesis of the ss-PCM were 1-dodecylamine (98%) (Nº CAS 124-22-1) from Acros organics B.V.B.A, copper (II) chloride dehydrated (Nº CAS 10125-13-0) from VWR international and hydrochloric acid 37% (Nº CAS 7647-01-0) from Labbox.

2.2. Synthesis procedure

The synthesis and recrystallization procedures are presented in Fig. 1. To evaluate the solvents, a solution of dodecylamine (3.7 g, 20 mmol) in MeOH, EtOH or IspOH (45 mL) was placed in a round-bottom flask containing $CuCl_2 \cdot 2H_2O$ (1.7 g, 10 mmol) at room temperature. Then a solution of HCl (1.7 mL, 20 mmol) in MeOH, EtOH, or IspOH (5 mL) was added dropwise through the condenser under magnetic stirring. The final molar ratio of the reagents $C_{12}H_{27}N$:HCl:$CuCl_2 \cdot 2H_2O$ was 2:2:1. The mixture was refluxed at 337 K for 4 h with vigorous and constant stirring. After this time, the heat source was removed, and the solution was allowed to stand for one day. The resulting solid was filtered under a vacuum to obtain a crude precipitate (S1). The solvent of the filtrate solution (residual water, RW) was removed and dried on a rotary evaporator to obtain a new solid (RW1). Subsequent crystallizations of S1 were carried out by adding ~15 mL (required amount) of solvent to dissolve the product. The mixture was then refluxed at 337 K for 45 min. Following the same procedure, the solution was left in a round bottom flask for one day to crystallize. It was then filtered to obtain a new solid (S2) and residual water (RW2). The recrystallization procedure was repeated twice to obtain S3, S4, RW3 and RW4 [26]. For the evaluation of the solvents for recrystallization, the same procedure was carried out using IspOH as the solvent for the recrystallization step.

To increase the yield of the synthesis, an alternative synthesis approach (method D) without filtration and recrystallization steps was evaluated. In this alternative procedure, shown in grey in Fig. 1, the solution is poured into a Petri dish after being refluxed at 337 K for 4 h and dried in a desiccator for 7 days.

2.3. Characterization

The crystal and chemical structure, the phase transition and the specific heat of all solids obtained were analyzed to determine the optimal synthesis route in terms of stability and latent heat. In addition, the residual water samples (RW2, RW3 and RW4) were dried by rotatory evaporation, and the chemical structure, as well as the phase transition, were analyzed to evaluate the efficiency of the recrystallization steps. It is important to note that the solid MetOH S4 did not precipitate, so it was obtained by rotatory evaporation. As a result, no MetOH RW 4 was obtained. In 2addition, the reaction yield and mass loss due to the recrystallization process were evaluated to determine the optimal synthesis route.

2.3.1. Morphology

A scanning electron microscope (SEM) was used to examine the morphology of the synthesized structures, using an XTE 325/D8395, Quanta 200 FEI. Several representative flakes were selected and attached to a carbon adhesive and coated with carbon to acquire SEM images and perform energy-dispersive scattering (EDS) analysis of the surface.

2.3.2. Crystal structure characterization

The structure of the resulting samples was determined by X-ray powder diffraction (XRD) (PANalytical X'Pert PRO MPD). The tests were done with Cu Kα radiation ($\lambda = 1.5418$ Å), a voltage of 45 kV and a tube current of 40 mA. The measurements were obtained in continuous scan mode and the 2θ range from 1° to 40° with a step size of 0.026° 2θ and a measuring time of 300 s per step.

2.3.3. Chemical structure characterization

Fourier transform infrared spectroscopy (FTIR) combined with attenuated total reflectance (ATR) (Perkin Elmer Spectrum Two™) was used to determine the molecular structures and analyze the chemical changes that occurred during the synthesis. The FTIR measurements were performed on a KBr disc at room temperature.

2.3.4. Phase transition characterization

The thermophysical properties of the resulting samples were investigated using differential scanning calorimetry (DSC) (Mettler Toledo DSC 822e Star 3+). The phase transition temperature (T_t) and enthalpy (ΔH) were evaluated between 303 K and 353 K with a heating rate of 1 K/min and a nitrogen flow of 50 ml/min. Each analysis was repeated three times, the first analysis being discarded due to contact issues between the sample and the crucible.

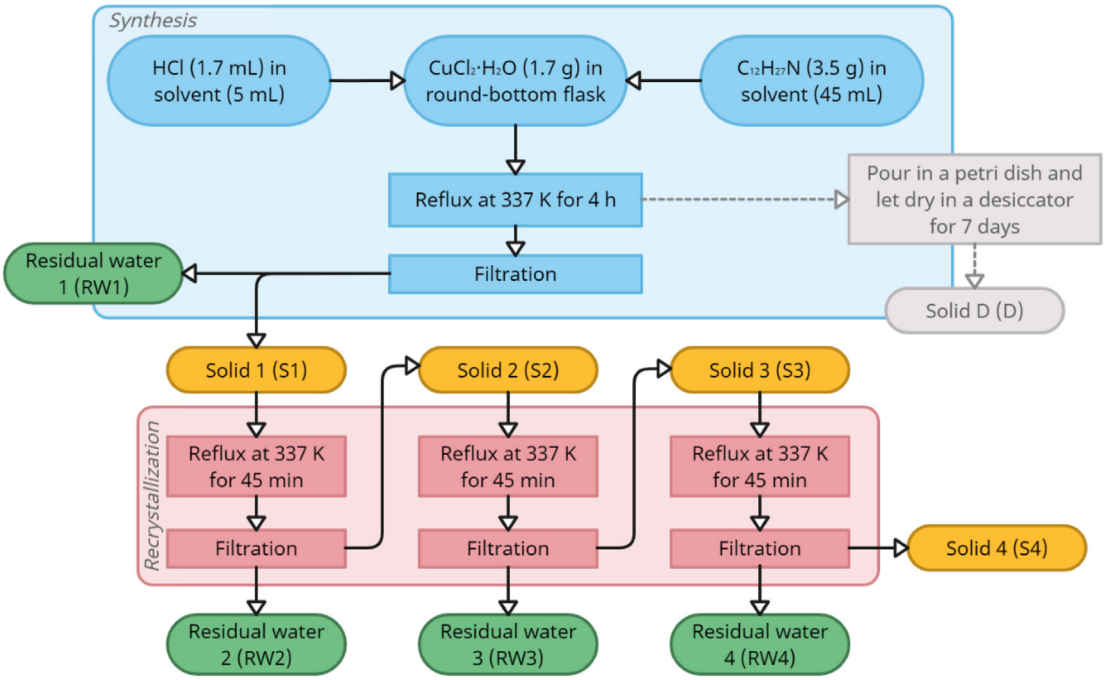

Fig. 1. Diagram of the synthesis procedure.

Table 1
Reaction yield and mass loss of the different syntheses.

	MetOH	EtOH	IspOH	MetOH-IspOH	EtOH-IspOH	MetOH_D	EtOH_D	IspOH_D
S1, yield (%)	66.28	73.62	85.61	67.12	75.96	88.28	89.36	95.24
S2, mass loss (%)	43.72	12.60	4.26	8.99	4.38	–	–	–
S3, mass loss (%)	65.37	15.38	4.17	24.51	7.71	–	–	–
S4, mass loss (%)	–	10.81	3.85	4.75	6.15	–	–	–

2.3.5. Specific heat capacity

DSC was used to determine the specific heat (C_p) at 313 K, 323 K, 333 K, 343 K, and 353 K using the approach established by Ferrer et al. [27]. His approach, the sapphire is analyzed as an internal standard and the sample is analyzed in successive isothermal segments, without heating ramps and with a temperature

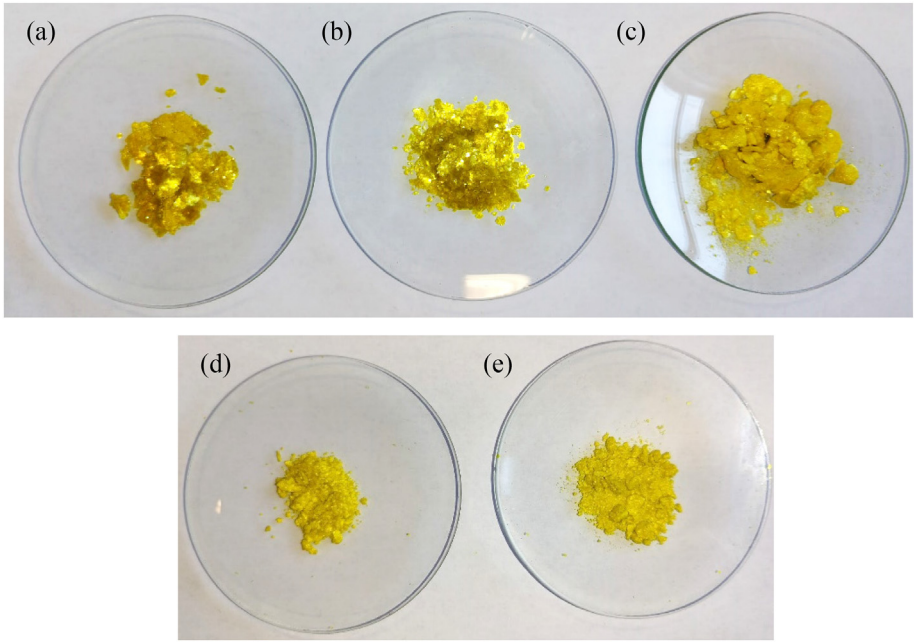

Fig. 2. Images of the solids obtained; (a) is MetOH_S3, (b) is EtOH_S4, (c) is IspOH_S4, (d) MetOH-IspOH_S4 and (e) EtOH-IspOH_S4.

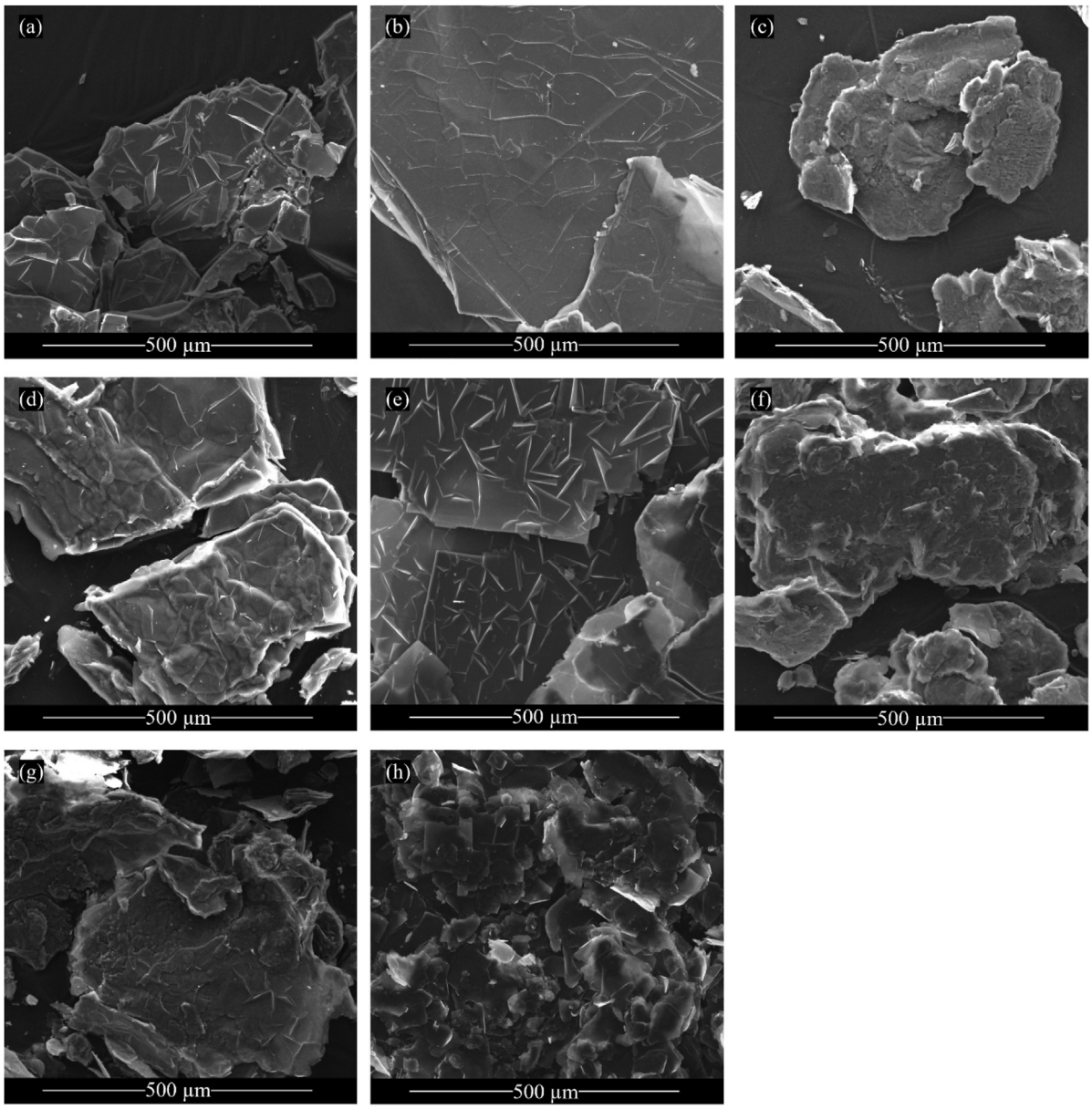

Fig. 3. SEM images of the main solids obtained; (a) MetOH_S3, (b) MetOH_D, (c) MetOH-IspOH_S4, (d) EtOH_S4, (e) EtOH_D, (f) EtOH-IspOH_S4, (g) IspOH_S4 and (h) IspOH_D.

difference between the isothermal steps of 1 K. The heat difference between the isothermal steps is represented by heat flow peaks. By integrating these peaks on the sapphire and the sample, the C_p value is calculated using Eqs. (1) and (2).

$$A_s = \frac{\dot{Q}_s}{m_s} = C_{ps} \cdot \beta \tag{1}$$

$$A_m = \frac{\dot{Q}_m}{m_m} = C_{pm} \cdot \beta \tag{2}$$

Where A [J/g] is the integrated area, $\dot{Q}$ [mW] is the heat flux, m [mg] is the mass of the sample and β [K/min] is the heating rate, and the sub-indices s and m correspond to the sapphire and sample, respectively. Since the C_p of the sapphire is known and all required parameters are known, the C_p of the sample material can be calculated with Eq. (3).

$$C_{pm} = \frac{C_{pm} \cdot A_m}{A_s} \tag{3}$$

3. Results and discussion

3.1. Reaction yield obtained and mass loss

The reaction yield and mass loss during the recrystallization of the different synthesis routes are shown in Table 1. The higher reaction yield is obtained with the synthesis method D, which does not require a filtration or recrystallization step, thus the solid is obtained directly by solvent evaporation. The following higher reaction yield is obtained when synthesizing with the isopropanol, followed by the ethanol and, finally methanol. This behavior is related to the solubility of CuC_{12} in the different solvents. Indeed, this component is more soluble in methanol than in isopropanol, as shown by the mass loss in the recrystallization steps (Table 1).

3.2. Morphology study

Clear differences can be seen in the morphology of the solid obtained, as shown in Fig. 2. The solid produced by the direct method has similar morphology with MetOH, EtOH and IspOH. It can be seen that MetOH_S3 and EtOH_S4 have comparable morphologies that resemble flakes, while IspOH_S4, MetOH-IspOH_S4 and EtOH-IspOH_S4 have similar morphology that is powdery. These morphological differences could be related to a decrease in the crystallinity of the solids, which could be reflected in the transition enthalpy values.

In addition, a secondary electron microscope was used to thoroughly examine the morphology of the solids obtained (Fig. 3). MetOH_S3, MetOH_D, EtOH_S4 and EtOH_D exhibited similar morphology reminiscent of two-dimensional crystals. The samples prepared with isopropanol under reflux IspOH_S4, Met-Isp_S4 and Et-Isp_S4 appear to be more of an aggregation with lower crystallinity. However, the IspOH_D has a morphology somewhere in between the two, with some crystalline crystals and aggregates.

3.3. Crystal structure analysis

The experimental XRD results of the CuC_{12} obtained with the different solvents are shown in Fig. 4. The diffraction peaks at 6°, 9°, 12°, etc. Prove the formation of a layered crystalline structure as each peak is related to the reflections of the (00*l*) [l = 1,2,3, …] planes, which are strongly oriented along the c-axis [20,28–30].

The main peaks obtained in the XRD diffractograms are related to the CuC12. However, in some cases, the unreacted material is detected. Some extra peaks related to unreacted reactants are detected in some of the structures. The peaks at 16.14° and 21.90° 2θ correspond to the two more intense peaks of $CuCl_2{\cdot}2HO_2$ and the peaks at 9.90°, 14.90°, 22.50° and 29.40° 2θ correspond to the alkylamine ($C_{12}H_{24}N_2$) [31,32]. Unreacted $CuCl_2{\cdot}2HO_2$ and $C_{12}H_{24}N_2$ are mainly detected in RW samples. Also, in EtOH_S4 and EtOH_D is able to see that some $CuCl_2{\cdot}2HO_2$ is unreacted. Despite this, the main peaks of the RW sample are related to the main structure, illustrating that some of the synthesized components remain in the solution after the recrystallization process.

3.4. Chemical structure analysis

The FT-IR spectra of the different samples of CuC_{12} are shown in Fig. 5. All samples show a similar FT-IR spectrum.

The bands associated with the amine functional group are: 3400-3250 cm^{-1} bands assigned to the stretching vibration of N–H, 1581 cm^{-1} assigned to the asymmetric deformation of $R{-}NH_3^+$ of the primary amine salt, and the symmetric deformation of $R{-}NH_3^+$ band corresponds to the 1491 and 1480 cm^{-1} bands, 1215 cm^{-1} band of C–N stretching and 769 cm^{-1} bands of $R{-}NH_3^+$ wagging [15,28]. The bands associated with the carbon chain are: 2955, 2871, 2917 and 2849 cm^{-1} bands are the asymmetric and symmetric stretching of $R{-}CH_3$ and $R{-}CH_2{-}R$, respectively [28]. The 1472 and 1463 cm^{-1} are related to the bending of $R{-}CH_2{-}R$. The band at 1377 cm^{-1} is assigned to the symmetric bending of $R{-}CH_3$. The bands at 728 and 720 cm^{-1} for $R{-}CH_2{-}R$ rocking and the bands at 891 cm^{-1} for the terminal C–C stretching [15,28,33,34].

In the FT-IR spectra, some bands are non-localized vibration modes, where the frequency and intensity of these bands depend on the chain length and conformation, and localized modes, where the frequency depends only on the local conformation and is practically independent of the chain length [33]. The non-localized modes are the $R{-}CH_2{-}R$ bending which appears at 1472 and 1463 cm^{-1}, and the $R{-}CH_2{-}R$ rocking vibrations at 728 and 720 cm^{-1}, but which normally appear around 1453 cm^{-1} and 730 cm^{-1}, respectively.

In addition, the splitting of some bands, $R{-}NH_3^+$ symmetric deformation, $R{-}CH_2{-}R$ bending, and $R{-}CH_2{-}R$ rocking was detected. The origin of the band splitting is based on the intermolecular coupling due to the dipole-dipole interaction between the C–H bonds and the short range of the repulsive force between the two nearest hydrogen bonds [34].

3.5. Phase transition analysis

Bis-alkylammonium tetrachlorometallates are known to exhibit a variety of structural phase transitions determined by the dynamics of the alkylammonium group and the rotation of the chlorometallates. For alkylammonium, there are two types of phases: (1) order-disorder of the rigid alkylammonium chain and

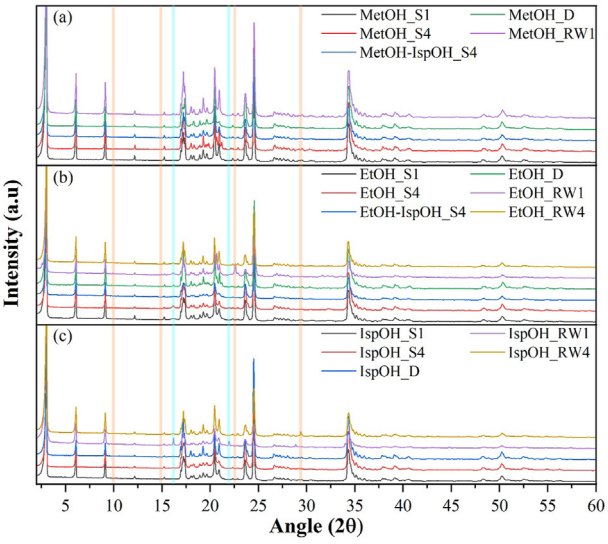

Fig. 4. XRD diffractograms of the samples in different synthesis and recrystallization solvents at different recrystallization steps.

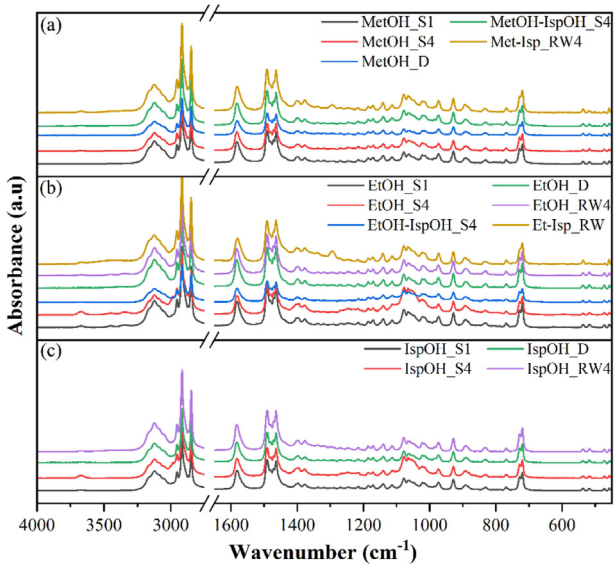

Fig. 5. Infrared spectra of samples in different synthesis and recrystallization solvents at different recrystallization steps.

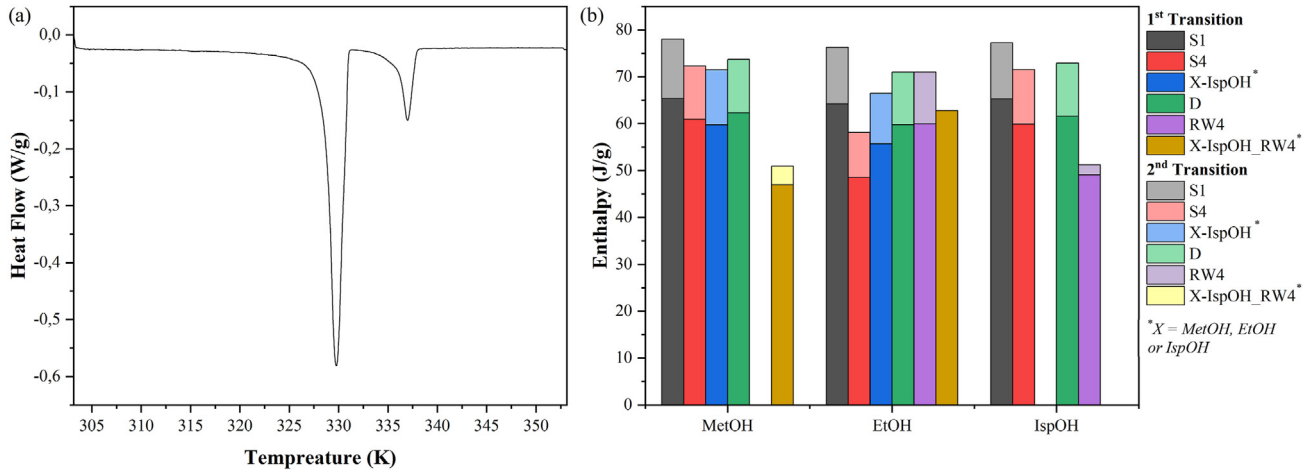

Fig. 6. (a) Heat flow signal vs temperature of the MetOH_S4 sample; (b) Enthalpy of the first and second transitions of the samples in different synthesis, recrystallization, and residual water.

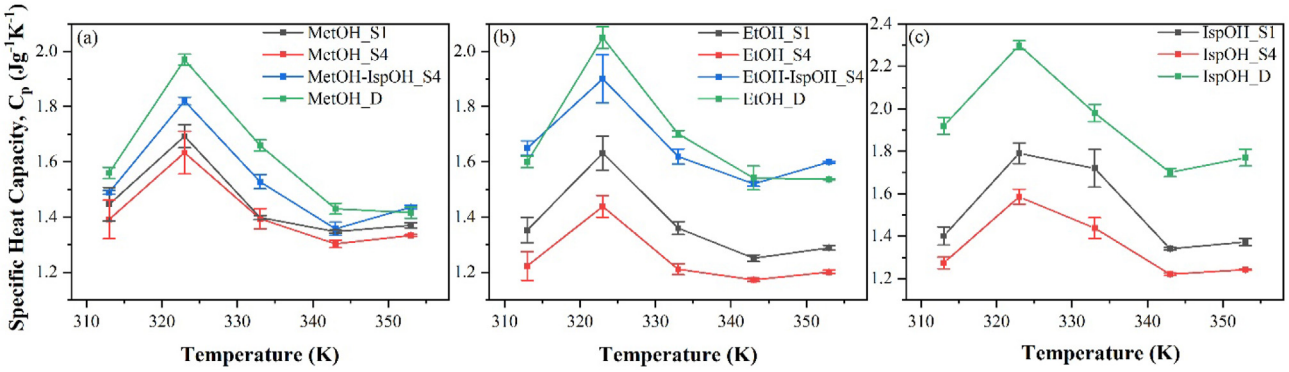

Fig. 7. Specific heat of the samples in different synthesis solvents before and after the recrystallization steps.

(2) conformational transition "partial melting" of the hydrocarbon chain; this second phase only occurs when the hydrocarbon chain contains ≥4 carbons [33]. CuC_{12} shows two solid state transitions at 329.15 K and 336.15 K with an associated ΔH of 72 and 12 J/g, respectively. The transition at 329.15 K corresponds to type (1) and at 336.15 K to type (2) of phase transitions, see Fig. 6 (a) [35].

Relative differences in ΔH are found in the different products obtained in each step of the synthesis procedure see Fig. 6 (b). In all cases, the first product obtained (S1) is the one with a higher ΔH in the first transition. This is due to the higher crystallinity of the product in the first step of the synthesis. The following products obtained have a lower ΔH after the recrystallization step: part of the crystallinity of the product is therefore lost during this process. No differences were found with respect to the solvent. As expected, the sample MetOH-Isp_S4 shows lower enthalpy values than MetOH_S4 and EtOH-IspOH_S4 shows higher values than EtOH_S4. This is due to the differences in crystal growth in the different media. In addition, the samples synthesized by method D have lower enthalpy than the S1 samples. Better crystals are obtained when a slower cooling rate is applied, which is the case when synthesizing in a round-bottom flask, as the residual heat of the aluminium reaction block is released slowly. In contrast, a fast cooling rate is obtained when the product is poured into a Petri dish directly after the synthesis (Method D).

With respect to the RW samples, these solids present the two solid state transition characteristics of CuC_{12}. Lower enthalpy values are obtained than for the S1 sample, which can be attributed to a lower crystallinity of the component, which could be due to the use of the rotatory evaporator.

3.6. Heat capacity

The specific heat of the samples was measured between 313 K and 353 K, see Fig. 7. All samples present a similar profile of specific heat as a function of temperature, with a maximum Cp value at 323 K, which is due to the proximity of the main polymorphic transition of this compound. It is noticeable that the samples synthesized by method D show higher Cp values. The difference in Cp could be due to differences in crystallinity between the samples or the presence of residual solvent as an impurity.

4. Conclusions

In this study, the CuC_{12} organometallic layered perovskite phase change material was successfully synthesized by two different synthesis procedures and with three different solvent media and recrystallization media (MetOH, EtOH and IspOH). A total of 21 samples were evaluated, eight of which were the product of the residual water obtained.

It was found that the structure of the compound does not change with the solvent or the recrystallisation media, as shown by the XRD and FTIR results. However, some unreacted reactants were found on EtOH_S4 and EtOH_D. In terms of reaction yield and specific heat capacity, better results are obtained with the non-

filtered and non-recrystallized method (Method D), which has higher of specific heat values. However, no significant differences were found in the enthalpy values between the different methods. As for the recrystallization products (RW), the presence of the compound was observed in the XRD and FTIR results, implying that the recrystallization process reduces the yield of the synthesis. Although, some unreacted reactants were detected in the XRD in the RW samples. It is concluded that for thermal energy storage purposes, method D is the optimal synthesis route to obtain CuC_{12} organometallic layered perovskite.

Furthermore, for the future use of this type of material in TES applications, thermal stability, cyclability, chemical compatibility with other materials, and in-situ validation should be investigated.

Authors' contributions

R. Salgado: Conceptualization, Methodology, Formal analysis, Investigation, Data curation, Writing - original draft, Writing - review & editing, Visualization. **C. Barreneche:** Supervision, Writing - Review & editing, Funding acquisition. **A. I. Fernández:** Conceptualization, Supervision, Visualization, Writing - Review & editing, Funding acquisition.

Declaration of competing interest

The authors declare that they have no known competing financial interests or personal relationships that could have appeared to influence the work reported in this paper.

Data availability

Data will be made available on request.

Acknowledgements

The authors would like to thank the Catalan Government for the quality accreditation given to their research group DIOPMA (2017 SGR 0118, 2021 SGR 00708). DIOPMA is a certified agent TECNIO in the category of technology developers from the Government of Catalonia. The authors are grateful to the CCiTUB for the equipment or measurements of XRD and to the Prof. Jordi García of the Department of Inorganic and Organic Chemistry of the Universitat de Barcelona.

This work was partially supported by the grant RTI2018-093849-B-C32 and PID2021-123511OB-C32 funded by MCIN/AEI/10.13039/501100011033 and, as appropriate, by "ERDF A way of making Europe", and R. Salgado-Pizarro PhD grant PRE2019-087336 funded by MCIN/AEI/10.13039/501100011033 and, as appropriate, by "ESF Investing in your future".

References

[1] M. Mastani Joybari, F. Haghighat, J. Moffat, P. Sra, Heat and cold storage using phase change materials in domestic refrigeration systems: the state-of-the-art review, Energy Build. 106 (2015) 111–124, https://doi.org/10.1016/j.enbuild.2015.06.016.

[2] A. Sciacovelli, M.E. Navarro, Y. Jin, G. Qiao, L. Zheng, G. Leng, L. Wang, Y. Ding, High density polyethylene (HDPE) — graphite composite manufactured by extrusion: a novel way to fabricate phase change materials for thermal energy storage, Particuology 40 (2018) 131–140, https://doi.org/10.1016/j.partic.2017.11.011.

[3] N. Putra, S. Rawi, M. Amin, E. Kusrini, E.A. Kosasih, T.M. Indra Mahlia, Preparation of beeswax/multi-walled carbon nanotubes as novel shape-stable nanocomposite phase-change material for thermal energy storage, J. Energy Storage 21 (2019) 32–39, https://doi.org/10.1016/j.est.2018.11.007.

[4] K. Pielichowska, K. Pielichowski, Phase change materials for thermal energy storage, Prog. Mater. Sci. 65 (2014) 67–123, https://doi.org/10.1016/j.pmatsci.2014.03.005.

[5] R. Salgado-Pizarro, G. Ulldemolins, M.E. Navarro, A. Palacios, A. Calderón, Y. Ding, A.I. Fernández, C. Barreneche, New shape-stabilized phase change materials obtained by single-screw extruder, Energy Storage 3 (2021), https://doi.org/10.1002/est2.268.

[6] R. Salgado-Pizarro, J.A. Padilla, E. Xuriguera, C. Barreneche, A.I. Fernández, Novel shape-stabilized phase change material with cascade character: synthesis, performance and shaping evaluation, Energies 14 (2021) 2621, https://doi.org/10.3390/en14092621.

[7] C. Barreneche, L. Navarro, A. de Gracia, A.I. Fernández, L.F. Cabeza, In situ thermal and acoustic performance and environmental impact of the introduction of a shape-stabilized PCM layer for building applications, Renew. Energy 85 (2016) 281–286, https://doi.org/10.1016/j.renene.2015.06.054.

[8] O. Pons, A. Aguado, A.I. Fernández, L.F. Cabeza, J.M. Chimenos, Review of the use of phase change materials (PCMs) in buildings with reinforced concrete structures, Mater. Construcción 64 (2014) e031, https://doi.org/10.3989/mc.2014.05613.

[9] M. Pomianowski, P. Heiselberg, R.L. Jensen, R. Cheng, Y. Zhang, A new experimental method to determine specific heat capacity of inhomogeneous concrete material with incorporated microencapsulated-PCM, Cement Concr. Res. 55 (2014) 22–34, https://doi.org/10.1016/j.cemconres.2013.09.012.

[10] V. Busico, P. Corradini, M. Vacatello, F. Fittipaldi, L. Nicolais, Solid-solid phase transitions for thermal energy storage, in: C. den Duden (Ed.), Thermal Storage of Solar Energy, Springer Netherlands, Dordrecht, 1981, pp. 309–324, https://doi.org/10.1007/978-94-009-8302-1_30.

[11] A. Fallahi, G. Guldentops, M. Tao, S. Granados-Focil, S. van Dessel, Review on solid-solid phase change materials for thermal energy storage: molecular structure and thermal properties, Appl. Therm. Eng. 127 (2017) 1427–1441, https://doi.org/10.1016/j.applthermaleng.2017.08.161.

[12] C.R. Raj, S. Suresh, R.R. Bhavsar, V.K. Singh, Recent developments in thermophysical property enhancement and applications of solid solid phase change materials, J. Therm. Anal. Calorim. 139 (2020) 3023–3049, https://doi.org/10.1007/s10973-019-08703-w.

[13] G.F. Needham, R.D. Willett, H.F. Franzen, Phase transitions in crystalline models of bilayers. 1. Differential scanning calorimetric and x-ray studies of $(C_{12}H_{25}NH_3)_2MCl_4$ and $(C_{14}H_{29}NH_3)_2MCl_4$ salts (M = Mn^{2+}, Cd^{2+}, Cu^{2+}), J. Phys. Chem. 88 (1984) 674–680, https://doi.org/10.1021/j150648a012.

[14] V. Busico, C. Carfagna, V. Salerno, M. Vacatello, F. Fittipaldi, The layer perovskites as thermal energy storage systems, Sol. Energy 24 (1980) 575–579, https://doi.org/10.1016/0038-092X(80)90356-4.

[15] J.-K. Kang, J.-H. Choy, M. Rey-Lafon, Phase transition behavior in the perovskite-type layer compound $(n\text{-}C_{12}H_{25}NH_3)_2CuCl_4$, J. Phys. Chem. Solid. 54 (1993) 1567–1577, https://doi.org/10.1016/0022-3697(93)90351-Q.

[16] W. Li, D. Zhang, T. Zhang, T. Wang, D. Ruan, D. Xing, H. Li, Study of solid–solid phase change of $(n\text{-}C_nH_{2n+1}NH_3)_2MCl_4$ for thermal energy storage, Thermochim. Acta 326 (1999) 183–186, https://doi.org/10.1016/S0040-6031(98)00497-3.

[17] C.R. Raj, S. Suresh, R.R. Bhavsar, V.K. Singh, A.S. Reddy, A. Upadhyay, Manganese-based layered perovskite solid–solid phase change material: synthesis, characterization and thermal stability study, Mech. Mater. 135 (2019) 88–97, https://doi.org/10.1016/j.mechmat.2019.05.004.

[18] E. Landi, M. Vacatello, New disordered polymorphs in long chain alkylammonium tetrachlorocobaltates(II), Thermochim. Acta 12 (1975) 141–146, https://doi.org/10.1016/0040-6031(75)85021-0.

[19] V. Busico, C. Carfagna, V. Salerno, M. Vacatello, Thermal behavior of complexes of general formula $(n\text{-}C_nH_{2n+1}NH_2)_2CuCl_2$, Thermochim. Acta 39 (1980) 1–5, https://doi.org/10.1016/0040-6031(80)80051-7.

[20] D. He, Y. Di, Y. Yao, Y. Liu, W. Dan, Crystal structure, low-temperature heat capacities, and thermodynamic properties of bis(dodecylammonium) tetrachlorocuprate $(C_{12}H_{28}N)_2CuCl_4$ (s), J. Chem. Eng. Data 55 (2010) 5739–5744, https://doi.org/10.1021/je100699g.

[21] Z. Zhi Ying, Y. Meng Lin, Thermodynamic properties and phase transitions of dodecylammonium tetrachloromanganate(II) and tetrachlorozincate(II) from 280 to 500 K, Thermochim. Acta 123 (1988) 15–22, https://doi.org/10.1016/0040-6031(88)80005-4.

[22] Y. Kong, Y. Di, W. Yang, Y. Lü, Z. Tan, Crystal structure, phase transition, and thermodynamic properties of bis-dodecylammonium tetrachlorozincate $(C_{12}H_{25}NH_3)_2ZnCl_4$(s), Chin. J. Chem. 28 (2010) 521–530, https://doi.org/10.1002/cjoc.201090106.

[23] C.F. Gao, L.P. Wang, Q.F. Li, C. Wang, Z.D. Nan, X.Z. Lan, Tuning thermal properties of latent heat storage material through confinement in porous media: the case of $(1\text{-}C_nH_{2n+1}NH_3)_2ZnCl_4$ (n=10 and 12), Sol. Energy Mater. Sol. Cell. 128 (2014) 221–230, https://doi.org/10.1016/j.solmat.2014.05.019.

[24] M.M. Abdel-Kader, A.I. Aboud, W.M. Gamal, Characterization of organic–inorganic hybrid layered perovskite and intercalated compound $(n\text{-}C_{12}H_{25}NH_3)_2ZnCl_4$, Phase Transitions 89 (2016) 448–470, https://doi.org/10.1080/01411594.2015.1077957.

[25] E. Landi, M. Vacatello, Metal-dependent thermal behaviour in $(n\text{-}C_nH_{2n+1}NH_3)_2MCl_4$, Thermochim. Acta 13 (1975) 441–447, https://doi.org/10.1016/0040-6031(75)85084-2.

[26] F. Kuznik, K. Johannes, Thermodynamic efficiency of water vapor/solid chemical sorption heat storage for buildings: theoretical limits and integration considerations, Appl. Sci. 10 (2020) 489, https://doi.org/10.3390/app10020489.

[27] G. Ferrer, C. Barreneche, A. Solé, I. Martorell, L.F. Cabeza, New proposed methodology for specific heat capacity determination of materials for thermal

energy storage (TES) by DSC, J. Energy Storage 11 (2017) 1–6, https://doi.org/10.1016/j.est.2017.02.002.

[28] M. Bochalya, P.K. Kanaujia, G. Vijaya Prakash, S. Kumar, Structural and optical diversity in copper halide-based ferromagnetic inorganic-organic layered hybrids, J. Solid State Chem. 273 (2019) 219–225, https://doi.org/10.1016/j.jssc.2019.03.012.

[29] M. Bochalya, G.V. Prakash, S. Kumar, Magnetism and phase segregation in two-dimensional inorganic-organic $(C_{12}H_{25}NH_3)_2Cu_{1-y}Mn_yCl_4$ hybrids, J. Solid State Chem. 273 (2019) 32–36, https://doi.org/10.1016/j.jssc.2019.02.025.

[30] M. Bochalya, P.K. Kanaujia, G.V. Prakash, S. Kumar, Structural phase transitions and thermal stability in Cu-based 2D inorganic-organic hybrid perovskite systems, in: AIP Conf Proc, American Institute of Physics Inc., 2019, 030001, https://doi.org/10.1063/1.5122329.

[31] Å. Engberg, L.-I. Staffansson, An X-ray refinement of the crystal structure of copper(II) chloride dihydrate, Acta Chem. Scand. 24 (1970) 3510–3526, https://doi.org/10.3891/acta.chem.scand.24-3510.

[32] Y.-X. Kong, Y.-Y. Di, Y.-Q. Zhang, W.-W. Yang, Z.-C. Tan, Crystal structure and thermochemical properties of 1-dodecylamine hydrochloride ($C_{12}H_{28}NCl$) (s), Thermochim. Acta 495 (2009) 33–37, https://doi.org/10.1016/j.tca.2009.05.015.

[33] L. Ricard, M. Rey-Lafon, C. Biran, Vibrational study of the dynamics of n-decylammonium chains in the perovskite-type layer compound decylammonium tetrachlorocadmate ($(C_{10}H_{21}NH_3)_2CdCl_4$), J. Phys. Chem. 88 (1984) 5614–5620, https://doi.org/10.1021/j150667a031.

[34] R.G. Snyder, Vibrational spectra of crystalline n-paraffins, J. Mol. Spectrosc. 7 (1961) 116–144, https://doi.org/10.1016/0022-2852(61)90347-2.

[35] J. Li, M. Barrio, D.J. Dunstan, R. Dixey, X. Lou, J.-L. Tamarit, A.E. Phillips, P. Lloveras, J. Li, D.J. Dunstan, R. Dixey, A.E. Phillips, X. Lou, M. Barrio, J.-L. Tamarit, P. Lloveras, Colossal reversible barocaloric effects in layered hybrid perovskite $(C_{10}H_{21}NH_3)_2MnCl_4$ under low pressure near room temperature, Adv. Funct. Mater. 31 (2021), 2105154, https://doi.org/10.1002/ADFM.202105154.